

Study the Higgs mass with the effective potential and Higgs decays in the $U(1)_X$ SSM

Shu-Min Zhao^{1,2*}, Xi Wang^{1,2}, Xing-Xing Dong^{1,2}, Hai-Bin Zhang^{1,2}, Tai-Fu Feng^{1,2,3}

¹ *Department of Physics, Hebei University, Baoding 071002, China*

² *Key Laboratory of High-precision Computation and Application of Quantum Field Theory of Hebei Province, Baoding 071002, China and*

³ *Department of Physics, Chongqing University, Chongqing 401331, China*

(Dated: September 16, 2022)

Abstract

As the $U(1)$ extension of the minimal supersymmetric standard model, the $U(1)_X$ SSM has new super fields such as right-handed neutrinos and three Higgs singlets. In the $U(1)_X$ SSM, the lightest CP-even Higgs mass m_{h^0} is researched through the Higgs effective potential with one loop corrections. We also calculate the Higgs decays $h^0 \rightarrow \gamma\gamma$, $h^0 \rightarrow VV$ ($V = W, Z$), $h^0 \rightarrow l\bar{l}Z$ and $h^0 \rightarrow \nu\bar{\nu}Z$. The obtained results are reasonable, which are in favour of the study of the Higgs characteristic and the phenomenology of the $U(1)_X$ SSM.

PACS numbers: 11.30.Er, 12.60.Jv, 14.80.Cp

Keywords: Higgs mass, effective potential, supersymmetry

* zhaosm@hbu.edu.cn

I. INTRODUCTION

In the standard model (SM) of particle physics, the Higgs boson is the last particle discovered and inherently related to the mechanism of spontaneous symmetry breaking (SSB). The observation of Higgs boson in 2012 [1] is a great success of the SM. Nevertheless, more detailed and precise investigations of Higgs are required and the search for new physics beyond the SM is one of the major issues of particle physics. On the other hand, the SM has some shortcomings, such as can not explain neutrino mass and mixing[2, 3], can not provide the candidates for cold dark matter, can not explain the asymmetry of matter and antimatter in the universe, etc..

A famous extension of the SM is the minimal supersymmetric extension of the standard model (MSSM)[4], which has been researched by physicists for several decades. People also extend MSSM into multiple models, in which the $U(1)$ extensions of MSSM are interesting. The $U(1)_X$ extension of MSSM is called as $U(1)_X$ SSM [5–7] with the local gauge group $SU(3)_C \times SU(2)_L \times U(1)_Y \times U(1)_X$. $U(1)_X$ SSM has more superfields (three Higgs singlets and right-handed neutrinos) than MSSM. The added right-handed neutrinos can not only explain the tiny mass of neutrino, but also provide a new dark matter candidate-light sneutrino. The μ problem appearing in the MSSM is relieved in the $U(1)_X$ SSM by the terms $\mu \hat{H}_u \hat{H}_d$ and $\lambda_H \hat{S} \hat{H}_u \hat{H}_d$ producing an effective $\mu_{eff} = \mu + \lambda_H v_S / \sqrt{2}$. The Higgs singlet S has a non-zero VEV ($v_S / \sqrt{2}$). The mixing of the CP-even parts of H_d , H_u , η , $\bar{\eta}$, S can improve the lightest CP-even Higgs mass at tree level.

Higgs pairs can be produced through gluon-gluon fusion [8, 9] in pp collision through loop diagrams. The Higgs boson mass and decays including $h^0 \rightarrow \gamma\gamma$ and $h^0 \rightarrow VV$ (with $V = Z, W$) have been studied in several models such as MSSM, NMSSM[10], B-LSSM[11], BLMSSM[12] and so on. In $U(1)_X$ SSM, we study the lightest CP-even Higgs mass through the Higgs effective potential with one loop corrections. The Higgs decays $h^0 \rightarrow \gamma\gamma$, $h^0 \rightarrow VV$ (with $V = Z, W$), $h^0 \rightarrow \bar{l}lZ$, $h^0 \rightarrow \nu_l \bar{\nu}_l Z$ (with $l = e, \mu, \tau$) are all calculated in this work.

For the decays h^0 to $\gamma\gamma$, ZZ and WW , the current values of the corresponding ratios $R_{\gamma\gamma}$, R_{ZZ} , R_{WW} are respectively $R_{\gamma\gamma} = 1.10 \pm 0.07$, $R_{WW} = 1.19 \pm 0.12$ and $R_{ZZ} = 1.01 \pm 0.07$ [13]. For the Higgs decays $h^0 \rightarrow \bar{l}lZ$, $h^0 \rightarrow \nu_l \bar{\nu}_l Z$ (with $l = e, \mu, \tau$)[14], they are in the reachable region of LHC. Some future experiments including two circular lepton

colliders(CEPC and FCC-ee)[15] and a linear lepton collider(ILC) have been proposed to study the properties of the Higgs boson. The accuracy of these colliders in measuring the Higgs decays will be improved obviously, and we believe that the decays $h^0 \rightarrow l\bar{l}Z$, $h^0 \rightarrow \nu_l\bar{\nu}_lZ$ (with $l = e, \mu, \tau$) can be detected in the near future.

In section 2, we briefly introduce the main content of $U(1)_X$ SSM and its superfields. The formulation for the Higgs effective potential and Higgs decays $h^0 \rightarrow \gamma\gamma$ (WW , ZZ), $h^0 \rightarrow l\bar{l}Z$, $h^0 \rightarrow \nu_l\bar{\nu}_lZ$ (with $l = e, \mu, \tau$) are shown in the section 3. We analytic the results numerically in the section 4, and obtain reasonable parameter space. The last section is used for the discussion and conclusion.

II. THE MAIN CONTENT OF $U(1)_X$ SSM

We extend MSSM with the local gauge group $U(1)_X$ to obtain $U(1)_X$ SSM, which has new super fields: three generation right-handed neutrinos and three Higgs singlets. Then $U(1)_X$ SSM can account for the data of neutrino oscillation. The introduction of three Higgs singlets (η , $\bar{\eta}$ and S) leads to the extension of mass squared matrix for CP-even Higgs. The new mixing of Higgs can improve the lightest CP-even Higgs mass at the tree level. One can find the particle contents in the work[6, 16].

In $U(1)_X$ SSM, the superpotential and soft SUSY breaking terms are shown here[6, 7, 16]

$$W = l_W \hat{S} + \mu \hat{H}_u \hat{H}_d + M_S \hat{S} \hat{S} - Y_d \hat{d} \hat{q} \hat{H}_d - Y_e \hat{e} \hat{l} \hat{H}_d + \lambda_H \hat{S} \hat{H}_u \hat{H}_d + \lambda_C \hat{S} \hat{\eta} \hat{\bar{\eta}} + \frac{\kappa}{3} \hat{S} \hat{S} \hat{S} + Y_u \hat{u} \hat{q} \hat{H}_u + Y_X \hat{\nu} \hat{\eta} \hat{\bar{\nu}} + Y_\nu \hat{\nu} \hat{l} \hat{H}_u. \quad (1)$$

$$\begin{aligned} \mathcal{L}_{soft} = & \mathcal{L}_{soft}^{MSSM} - B_S S^2 - L_S S - \frac{T_\kappa}{3} S^3 - T_{\lambda_C} S \eta \bar{\eta} + \epsilon_{ij} T_{\lambda_H} S H_d^i H_u^j \\ & - T_X^{IJ} \bar{\eta} \tilde{\nu}_R^{*I} \tilde{\nu}_R^J + \epsilon_{ij} T_\nu^{IJ} H_u^i \tilde{\nu}_R^{*I} \tilde{l}_j^J - m_\eta^2 |\eta|^2 - m_{\bar{\eta}}^2 |\bar{\eta}|^2 \\ & - m_S^2 S^2 - (m_{\tilde{\nu}_R}^2)^{IJ} \tilde{\nu}_R^{*I} \tilde{\nu}_R^J - \frac{1}{2} \left(M_S \lambda_{\tilde{X}}^2 + 2 M_{BB'} \lambda_{\tilde{B}} \lambda_{\tilde{X}} \right) + h.c. \end{aligned} \quad (2)$$

The two Higgs doublets and three Higgs singlets are

$$\begin{aligned} H_u &= \begin{pmatrix} H_u^+ \\ \frac{1}{\sqrt{2}}(v_u + \phi_u + iP_u^0) \end{pmatrix}, & H_d &= \begin{pmatrix} \frac{1}{\sqrt{2}}(v_d + \phi_d + iP_d^0) \\ H_d^- \end{pmatrix}, \\ \eta &= \frac{1}{\sqrt{2}}(v_\eta + \phi_\eta + iP_\eta^0), & \bar{\eta} &= \frac{1}{\sqrt{2}}(v_{\bar{\eta}} + \phi_{\bar{\eta}} + iP_{\bar{\eta}}^0), \\ S &= \frac{1}{\sqrt{2}}(v_S + \phi_S + iP_S^0). \end{aligned} \quad (3)$$

v_u , v_d , v_η , $v_{\bar{\eta}}$ and v_S respectively represent the VEVs of the Higgs superfields H_u , H_d , η , $\bar{\eta}$ and S . The definitions of two angles are $\tan \beta = v_u/v_d$ and $\tan \beta_\eta = v_{\bar{\eta}}/v_\eta$.

Y^Y denotes the $U(1)_Y$ charge and Y^X represents the $U(1)_X$ charge. One can write the covariant derivatives of $U(1)_X$ SSM in the form

$$D_\mu = \partial_\mu - i \begin{pmatrix} Y & X \end{pmatrix} \begin{pmatrix} g_Y & g'_{YX} \\ g'_{XY} & g'_X \end{pmatrix} \begin{pmatrix} A'_\mu{}^Y \\ A'_\mu{}^X \end{pmatrix}, \quad (4)$$

where $A'_\mu{}^Y$ and $A'_\mu{}^X$ denote the gauge fields of $U(1)_Y$ and $U(1)_X$ respectively.

It is convenient to perform a change of the basis with the rotation matrix R [17]

$$D_\mu = \partial_\mu - i \begin{pmatrix} Y^Y & Y^X \end{pmatrix} \begin{pmatrix} g_Y & g'_{YX} \\ g'_{XY} & g'_X \end{pmatrix} R^T R \begin{pmatrix} A'_\mu{}^Y \\ A'_\mu{}^X \end{pmatrix}, \quad (5)$$

$$\begin{pmatrix} g_Y & g'_{YX} \\ g'_{XY} & g'_X \end{pmatrix} R^T = \begin{pmatrix} g_1 & g_{YX} \\ 0 & g_X \end{pmatrix}, \quad R \begin{pmatrix} A'_\mu{}^Y \\ A'_\mu{}^X \end{pmatrix} = \begin{pmatrix} A_\mu^Y \\ A_\mu^X \end{pmatrix}. \quad (6)$$

In the end, the covariant derivatives of $U(1)_X$ SSM turn into

$$D_\mu = \partial_\mu - i \begin{pmatrix} Y^Y & Y^X \end{pmatrix} \begin{pmatrix} g_1 & g_{YX} \\ 0 & g_X \end{pmatrix} \begin{pmatrix} A_\mu^Y \\ A_\mu^X \end{pmatrix}. \quad (7)$$

In $U(1)_X$ SSM, the gauge bosons A_μ^X , A_μ^Y and V_μ^3 mix together at the tree level. We deduce their mass eigenvalues as

$$\begin{aligned} m_\gamma^2 &= 0, \\ m_{Z,Z'}^2 &= \frac{1}{8} \left((g_1^2 + g_2^2 + (g_{YX} + g_X)^2) v^2 + 4g_X^2 \xi^2 \right. \\ &\quad \left. \mp \sqrt{(g_1^2 + g_2^2 + (g_{YX} + g_X)^2) v^4 + 8((g_{YX} + g_X)^2 - g_1^2 - g_2^2) g_X^2 v^2 \xi^2 + 16g_X^4 \xi^4} \right). \end{aligned} \quad (8)$$

with $v^2 = v_u^2 + v_d^2$ and $\xi^2 = v_\eta^2 + v_{\bar{\eta}}^2$. Two mixing angles θ_W and θ'_W [7, 16] are used here.

Supposing μ , λ_H , λ_C , l_W , M_S , B_μ , L_S , T_κ , T_{λ_C} , T_{λ_H} , κ , B_S as real parameters, we show the simplified Higgs potential at tree level[6]

$$\begin{aligned} V_0 &= \frac{1}{2} g_X (g_X + g_{YX}) (|H_d^0|^2 - |H_u^0|^2) (|\eta|^2 - |\bar{\eta}|^2) + \lambda_H^2 |H_u^0 H_d^0|^2 + m_S^2 |S|^2 + l_W^2 \\ &\quad + \frac{1}{8} (g_1^2 + g_2^2 + (g_X + g_{YX})^2) (|H_d^0|^2 - |H_u^0|^2)^2 + \frac{1}{2} g_X^2 (|\eta|^2 - |\bar{\eta}|^2)^2 + \lambda_C^2 |\eta \bar{\eta}|^2 \\ &\quad + (\mu^2 + \lambda_H^2 |S|^2 + 2\text{Re}[\mu \lambda_H S]) (|H_d^0|^2 + |H_u^0|^2) + \lambda_C^2 |S|^2 (|\eta|^2 + |\bar{\eta}|^2) + m_\eta^2 |\eta|^2 \\ &\quad + 2\text{Re}[(l_W + 2M_S S^*)(\lambda_C \eta \bar{\eta} - \lambda_H H_u^0 H_d^0 + \kappa S^2)] + 4M_S^2 |S|^2 + \kappa^2 |S|^4 + m_{\bar{\eta}}^2 |\bar{\eta}|^2 \\ &\quad + 2\text{Re}[\lambda_C \kappa \eta^* \bar{\eta}^* S^2 + 2l_W M_S S - \lambda_C \lambda_H \eta^* \bar{\eta}^* H_u^0 H_d^0] + m_{H_u^0}^2 |H_u|^2 + m_{H_d}^2 |H_d|^2 \\ &\quad + 2\text{Re} \left[L_S S - H_d^0 H_u^0 (B_\mu + \lambda_H \kappa (S^2)^* + T_{\lambda_H} S) + \frac{1}{3} T_\kappa S^3 + T_{\lambda_C} \eta \bar{\eta} S + B_S S^2 \right]. \end{aligned} \quad (9)$$

The corresponding tadpole equations at tree level are also obtained in Ref.[6]. The tree level mass squared matrix for CP-even Higgs $(\phi_d, \phi_u, \phi_\eta, \phi_{\bar{\eta}}, \phi_s)$ is

$$M_{h,tree}^2 = \begin{pmatrix} m_{\phi_d\phi_d} & m_{\phi_u\phi_d} & m_{\phi_\eta\phi_d} & m_{\phi_{\bar{\eta}}\phi_d} & m_{\phi_s\phi_d} \\ m_{\phi_d\phi_u} & m_{\phi_u\phi_u} & m_{\phi_\eta\phi_u} & m_{\phi_{\bar{\eta}}\phi_u} & m_{\phi_s\phi_u} \\ m_{\phi_d\phi_\eta} & m_{\phi_u\phi_\eta} & m_{\phi_\eta\phi_\eta} & m_{\phi_{\bar{\eta}}\phi_\eta} & m_{\phi_s\phi_\eta} \\ m_{\phi_d\phi_{\bar{\eta}}} & m_{\phi_u\phi_{\bar{\eta}}} & m_{\phi_\eta\phi_{\bar{\eta}}} & m_{\phi_{\bar{\eta}}\phi_{\bar{\eta}}} & m_{\phi_s\phi_{\bar{\eta}}} \\ m_{\phi_d\phi_s} & m_{\phi_u\phi_s} & m_{\phi_\eta\phi_s} & m_{\phi_{\bar{\eta}}\phi_s} & m_{\phi_s\phi_s} \end{pmatrix}, \quad (10)$$

$$m_{\phi_d\phi_d} = m_{H_d}^2 + \mu^2 + \frac{1}{8} \left([g_1^2 + (g_X + g_{YX})^2 + g_2^2](3v_d^2 - v_u^2) + 2(g_{YX}g_X + g_X^2)(v_\eta^2 - v_{\bar{\eta}}^2) \right) + \sqrt{2}v_S\mu\lambda_H + \frac{1}{2}(v_u^2 + v_S^2)\lambda_H^2, \quad (11)$$

$$m_{\phi_d\phi_u} = -\frac{1}{4} \left(g_2^2 + (g_{YX} + g_X)^2 + g_1^2 \right) v_d v_u + \lambda_H^2 v_d v_u - \lambda_H l_W - \frac{1}{2} \lambda_H (v_\eta v_{\bar{\eta}} \lambda_C + v_S^2 \kappa) - B_\mu - \sqrt{2}v_S \left(\frac{1}{2} T_{\lambda_H} + M_S \lambda_H \right), \quad (12)$$

$$m_{\phi_u\phi_u} = m_{H_u}^2 + \mu^2 + \frac{1}{8} \left([g_1^2 + (g_X + g_{YX})^2 + g_2^2](3v_u^2 - v_d^2) + 2(g_{YX}g_X + g_X^2)(v_\eta^2 - v_{\bar{\eta}}^2) \right) + \sqrt{2}v_S\mu\lambda_H + \frac{1}{2}(v_d^2 + v_S^2)\lambda_H^2, \quad (13)$$

$$m_{\phi_d\phi_\eta} = \frac{1}{2} g_X (g_{YX} + g_X) v_d v_\eta - \frac{1}{2} v_u v_{\bar{\eta}} \lambda_H \lambda_C, \quad (14)$$

$$m_{\phi_u\phi_\eta} = -\frac{1}{2} g_X (g_{YX} + g_X) v_u v_\eta - \frac{1}{2} v_d v_{\bar{\eta}} \lambda_H \lambda_C, \quad (15)$$

$$m_{\phi_\eta\phi_\eta} = m_\eta^2 + \frac{1}{4} \left((g_{YX}g_X + g_X^2)(v_d^2 - v_u^2) + 2g_X^2(3v_\eta^2 - v_{\bar{\eta}}^2) \right) + \frac{\lambda_C^2}{2}(v_\eta^2 + v_S^2), \quad (16)$$

$$m_{\phi_d\phi_{\bar{\eta}}} = -\frac{1}{2} g_X (g_{YX} + g_X) v_d v_{\bar{\eta}} - \frac{1}{2} v_u v_\eta \lambda_H \lambda_C, \quad (17)$$

$$m_{\phi_u\phi_{\bar{\eta}}} = \frac{1}{2} g_X (g_{YX} + g_X) v_u v_{\bar{\eta}} - \frac{1}{2} v_d v_\eta \lambda_H \lambda_C, \quad (18)$$

$$m_{\phi_\eta\phi_{\bar{\eta}}} = (\lambda_C^2 - g_X^2) v_\eta v_{\bar{\eta}} + \frac{\lambda_C}{2} (2l_W - \lambda_H v_d v_u) + \frac{v_S}{\sqrt{2}} (2M_S \lambda_C + T_{\lambda_C}) + \frac{v_S^2}{2} \lambda_C \kappa, \quad (19)$$

$$m_{\phi_{\bar{\eta}}\phi_{\bar{\eta}}} = m_{\bar{\eta}}^2 + \frac{1}{4} \left((g_{YX}g_X + g_X^2)(v_u^2 - v_d^2) + 2g_X^2(3v_{\bar{\eta}}^2 - v_\eta^2) \right) + \frac{\lambda_C^2}{2}(v_{\bar{\eta}}^2 + v_S^2), \quad (20)$$

$$m_{\phi_d\phi_s} = \left(\lambda_H v_d v_S + \sqrt{2}v_d \mu - v_u (\kappa v_S + \sqrt{2}M_S) \right) \lambda_H - \frac{1}{\sqrt{2}} v_u T_{\lambda_H}, \quad (21)$$

$$m_{\phi_u\phi_s} = \left(\lambda_H v_u v_S + \sqrt{2}v_u \mu - v_d (\kappa v_S + \sqrt{2}M_S) \right) \lambda_H - \frac{1}{\sqrt{2}} v_d T_{\lambda_H}, \quad (22)$$

$$m_{\phi_\eta\phi_s} = \left(\lambda_C v_\eta v_S + v_{\bar{\eta}} (\kappa v_S + \sqrt{2}M_S) \right) \lambda_C + \frac{1}{\sqrt{2}} v_{\bar{\eta}} T_{\lambda_C}, \quad (23)$$

$$m_{\phi_{\bar{\eta}}\phi_s} = \left(\lambda_C v_{\bar{\eta}} v_S + v_\eta (\kappa v_S + \sqrt{2}M_S) \right) \lambda_C + \frac{1}{\sqrt{2}} v_\eta T_{\lambda_C}, \quad (24)$$

$$m_{\phi_s\phi_s} = m_S^2 + \left(2l_W + 3v_S(\kappa v_S + 2\sqrt{2}M_S) + \lambda_C v_\eta v_{\bar{\eta}} - \lambda_H v_d v_u\right)\kappa + 2B_S \\ + \frac{1}{2}\lambda_C^2\xi^2 + \frac{1}{2}\lambda_H^2v^2 + 4M_S^2 + \sqrt{2}v_S T_\kappa. \quad (25)$$

III. FORMULATION

The one loop effective potential can be written in the following form

$$V_{eff} = V_0 + V_1. \quad (26)$$

Here, V_1 is the potential from one loop correction. The concrete form of V_1 is [18–20]

$$V_1 = \sum_i \frac{n_i}{64\pi^2} m_i^4(\phi_d, \phi_u, \phi_\eta, \phi_{\bar{\eta}}, \phi_s) \left(\log \frac{m_i^2(\phi_d, \phi_u, \phi_\eta, \phi_{\bar{\eta}}, \phi_s)}{Q^2} - \frac{3}{2} \right). \quad (27)$$

We take the renormalization scale Q at TeV order. The degrees of freedom for each mass eigenstate are represented by n_i (-12 for quarks, -4 for leptons and charginos, -2 for neutralinos and neutrinos, 6 for squarks, 2 for sleptons and charged Higgs, 3 and 6 for $Z(Z')$ and W bosons, 1 for sneutrinos and the neutral Higgs scalars).

Here, we use the conditions at one loop level through the following formula

$$\left\langle \frac{\partial V_{eff}}{\partial \phi_u} \right\rangle = \left\langle \frac{\partial V_{eff}}{\partial \phi_d} \right\rangle = \left\langle \frac{\partial V_{eff}}{\partial \phi_\eta} \right\rangle = \left\langle \frac{\partial V_{eff}}{\partial \phi_{\bar{\eta}}} \right\rangle = \left\langle \frac{\partial V_{eff}}{\partial \phi_s} \right\rangle = 0. \quad (28)$$

The corresponding analytic results are very tedious and we resolve the equations numerically. In order to save space in the text, we do not show the tedious analytic results here.

The mass squared matrix of CP-even Higgs is corrected by one loop contributions from the effective potential V_{eff}

$$M_h^2 = M_{h,tree}^2 + \Delta M_h^2. \quad (29)$$

The elements of the corrected mass squared matrix $M_{h,ij}^2$ can be deduced from the one loop effective potential V_{eff} through the following formula

$$M_{h,ij}^2 = \left\langle \frac{\partial^2 V_{eff}}{\partial \phi_i \partial \phi_j} \Big|_{\phi_i, \phi_j = \phi_d, \phi_u, \phi_\eta, \phi_{\bar{\eta}}, \phi_s} \right\rangle. \quad (30)$$

The lightest eigenvalue of M_h^2 should be the square of $m_{h^0} \simeq 125$ GeV.

The gluon fusion ($gg \rightarrow h^0$) [8, 9] chiefly produces h^0 at the LHC. With large Yukawa coupling, the virtual t quark loop is the dominate contribution during the one loop diagrams.

The large couplings of new particles can lead to considerable corrections

$$\Gamma_{NP}(h^0 \rightarrow gg) = \frac{G_F \alpha_s^2 m_{h^0}^3}{64\sqrt{2}\pi^3} \left| \sum_q g_{h^0 qq} A_{1/2}(x_q) + \sum_{\tilde{q}} g_{h^0 \tilde{q}\tilde{q}} \frac{m_Z^2}{m_{\tilde{q}}^2} A_0(x_{\tilde{q}}) \right|^2, \quad (31)$$

with $x_a = m_{h^0}^2/(4m_a^2)$. Here, q represents quark, and \tilde{q} denotes squark. The functions $A_{1/2}(x)$ and $A_0(x)$ are defined as

$$A_{1/2}(x) = 2 \left(x + (x-1)g(x) \right) / x^2, \quad A_0(x) = \left(g(x) - x \right) / x^2, \quad (32)$$

$$g(x) = \begin{cases} \arcsin^2 \sqrt{x}, & x \leq 1 \\ -\frac{1}{4} \left[\ln \frac{1+\sqrt{1-1/x}}{1-\sqrt{1-1/x}} - i\pi \right]^2, & x > 1. \end{cases} \quad (33)$$

The concrete expressions for $g_{h^0 qq}$ and $g_{h^0 \tilde{q}\tilde{q}}$ are

$$g_{h^0 \tilde{q}\tilde{q}} = \frac{-v}{m_q} C_{h^0 \tilde{q}\tilde{q}}, \quad g_{h^0 \tilde{q}\tilde{q}} = \frac{-S_W C_W}{em_Z} C_{h^0 \tilde{q}\tilde{q}}. \quad (34)$$

Here $S_W = \sin \theta_W$ and $C_W = \cos \theta_W$ with θ_W denoting the Weinberg angle. The coupling constants $C_{h^0 qq}$ and $C_{h^0 \tilde{q}\tilde{q}}$ are defined as

$$\mathcal{L} \supset C_{h^0 qq} (h^0 \bar{q}q) + C_{h^0 \tilde{q}\tilde{q}} (h^0 \tilde{q}\tilde{q}). \quad (35)$$

For the decay $h^0 \rightarrow \gamma\gamma$, the leading order contributions are from the one loop diagrams. Its decay width is written in the following form

$$\begin{aligned} \Gamma_{U(1)_X}(h^0 \rightarrow \gamma\gamma) &= \frac{G_F \alpha^2 m_{h^0}^3}{128\sqrt{2}\pi^3} \left| \sum_f N_c Q_f^2 g_{h^0 ff} A_{1/2}(x_f) + g_{h^0 H^\pm H^\pm} \frac{m_W^2}{m_{H^\pm}^2} A_0(x_{H^\pm}) \right. \\ &\quad \left. + g_{h^0 WW} A_1(x_W) + \sum_{i=1}^2 g_{h^0 \chi_i^\pm \chi_i^\pm} \frac{m_W}{m_{\chi_i}} A_{1/2}(x_{\chi_i}) + \sum_{\tilde{f}} N_c Q_{\tilde{f}}^2 g_{h^0 \tilde{f}\tilde{f}} \frac{m_Z^2}{m_{\tilde{f}}^2} A_0(x_{\tilde{f}}) \right|^2. \end{aligned} \quad (36)$$

The function $A_1(x)$ is defined as

$$A_1(x) = - \left[2x^2 + 3x + 3(2x-1)g(x) \right] / x^2. \quad (37)$$

The relevant couplings are defined in the following form

$$\begin{aligned} g_{h^0 WW} &= \frac{S_W}{em_W} C_{h^0 WW}, & g_{h^0 ZZ} &= \frac{C_W S_W}{em_Z} C_{h^0 ZZ}, \\ g_{h^0 \chi_i^\pm \chi_i^\pm} &= \frac{-2S_W}{e} C_{h^0 \chi_i^\pm \chi_i^\pm}^L, & g_{h^0 H^\pm H^\pm} &= \frac{-v}{2m_W^2} C_{h^0 H^\pm H^\pm}, \\ g_{h^0 \tilde{L}\tilde{L}} &= \frac{-S_W C_W}{em_Z} C_{h^0 \tilde{L}\tilde{L}}, \end{aligned} \quad (38)$$

$$\begin{aligned} \mathcal{L} &\supset C_{h^0 WW} g^{\mu\nu} h^0 W_\mu W_\nu + C_{h^0 ZZ} g^{\mu\nu} h^0 Z_\mu Z_\nu + C_{h^0 \tilde{L}\tilde{L}} h^0 \tilde{L}\tilde{L} \\ &\quad + \bar{\chi}_i^\pm (C_{h^0 \chi_i^\pm \chi_j^\pm}^L P_L + C_{h^0 \chi_i^\pm \chi_j^\pm}^R P_R) \chi_j^\pm h^0 + C_{h^0 H^\pm H^\pm} h^0 H^\pm H^\pm. \end{aligned} \quad (39)$$

The formulae for $h^0 \rightarrow ZZ$, WW are expressed as [21, 22]

$$\begin{aligned}\Gamma(h^0 \rightarrow WW) &= \frac{3e^4 m_{h^0}}{512\pi^3 S_W^4} |g_{h^0 WW}|^2 F\left(\frac{m_W}{m_{h^0}}\right), \\ \Gamma(h^0 \rightarrow ZZ) &= \frac{e^4 m_{h^0}}{2048\pi^3 S_W^4 C_W^4} |g_{h^0 ZZ}|^2 \left(7 - \frac{40}{3} S_W^2 + \frac{160}{9} S_W^4\right) F\left(\frac{m_Z}{m_{h^0}}\right).\end{aligned}\quad (40)$$

The concrete form of $F(x)$ is

$$\begin{aligned}F(x) &= -(1-x^2) \left(\frac{47}{2} x^2 - \frac{13}{2} + \frac{1}{x^2} \right) - 3(1-6x^2+4x^4) \ln x \\ &\quad + \frac{3(1-8x^2+20x^4)}{\sqrt{4x^2-1}} \cos^{-1} \left(\frac{3x^2-1}{2x^3} \right).\end{aligned}\quad (41)$$

We also study the processes of $h^0 \rightarrow \bar{l}lZ$ and $h^0 \rightarrow \bar{\nu}_l \nu_l Z$ (with $l = e, \mu, \tau$). The latter is simpler than the former, and can be obtained by taking the limit $m_l \rightarrow 0$ from the former, where m_l denotes the mass of lepton. For the processes of $h^0(p_1) \rightarrow l(p_2) + \bar{l}(p_3) + Z(p_4)$, the diagrams are shown in the Fig.1. The external particles all satisfy the on shell condition:

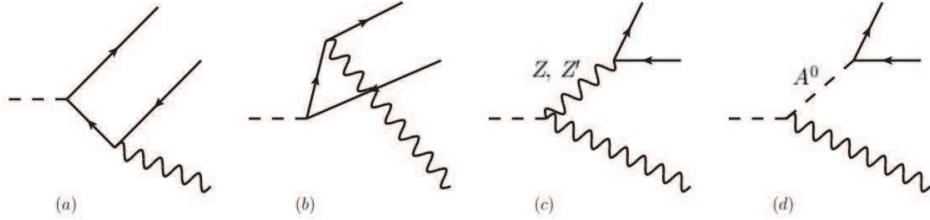


FIG. 1: The Feynman diagrams for $h^0 \rightarrow \bar{l}lZ$.

$p_1^2 = m_{h^0}^2$, $p_2^2 = p_3^2 = m_l^2$ and $p_4^2 = m_Z^2$. We use the Mandelstam invariants: $s = (p_2 + p_3)^2$, $t = (p_3 + p_4)^2$, $u = (p_2 + p_4)^2$ and $s + t + u = m_{h^0}^2 + 2m_l^2 + m_Z^2$. In our calculation, all lepton masses and the couplings of $\bar{l} - H^0(G^0) - l$ are kept.

From the diagrams in the Fig.1, we can obtain the decay through the following formula[14]

$$\Gamma(h^0 \rightarrow \bar{l}lZ) = \frac{1}{256\pi^3 m_{h^0}^3} \int_{4m_l^2}^{(m_{h^0}-m_Z)^2} ds \int_{t^-}^{t^+} \sum |\mathcal{M}|^2. \quad (42)$$

Here, \mathcal{M} is the Feynman amplitude for the Fig.1. The definitions of t^\pm are

$$t^\pm = \frac{1}{2} \left[m_{h^0}^2 + 2m_l^2 + m_Z^2 - s \pm \left(1 - \frac{4m_l^2}{s} \right)^{1/2} \left((m_{h^0}^2 + m_Z^2 - s)^2 - 4m_{h^0}^2 m_Z^2 \right)^{1/2} \right]. \quad (43)$$

IV. NUMERICAL RESULTS

To study the lightest CP-even Higgs h^0 mass ($m_{h^0} \simeq 125$ GeV) and h^0 decays $h^0 \rightarrow VV$ (with $V = \gamma, W, Z$), $h^0 \rightarrow l\bar{l}Z$ and $h^0 \rightarrow \nu_l\bar{\nu}_lZ$ (with $l = e, \mu, \tau$) in the $U(1)_X$ SSM, we consider the mass constraint for the Z' boson ($M_{Z'} > 5.1$ TeV)[23] from LHC experiments. The constraints $M_{Z'}/g_X \geq 6$ TeV[24] and $\tan\beta_\eta < 1.5$ [25] are also taken into account. The parameters are used to make the scalar lepton masses larger than 700 GeV, and chargino masses larger than 1100 GeV[26].

Some parameters are adopted here with $i = 1, 2, 3$

$$\begin{aligned} \kappa &= Y_{Xii} = 1, \quad v_S = 3.6 \text{ TeV}, \quad \mu = M_1 = T_{Dii} = 1 \text{ TeV}, \quad M_S = 2.7 \text{ TeV}, \\ \tan\beta_\eta &= 0.8, \quad B_\mu = B_S = M_{Lii}^2 = 1 \text{ TeV}^2, \quad l_W = 4 \text{ TeV}^2, \quad l_S = -300 \text{ TeV}^3, \\ T_\kappa &= 1.6 \text{ TeV}, \quad M_2 = 1.2 \text{ TeV}, \quad M_{BL} = 0.3 \text{ TeV}, \quad T_{Xii} = T_{Eii} = 0.5 \text{ TeV}, \\ T_{\nu ii} &= 0.8 \text{ TeV}, \quad M_{Eii}^2 = M_{Dii}^2 = 5 \text{ TeV}^2, \quad M_{\nu ii}^2 = 0.5 \text{ TeV}^2, \quad \xi = 17 \text{ TeV}. \end{aligned} \quad (44)$$

To simplify the numerical discussion, we use the following relations

$$T_{Uii} = T_u, \quad M_{Uii}^2 = M_U^2, \quad M_{Qii}^2 = M_Q^2, \quad (i = 1, 2, 3). \quad (45)$$

To explore the parameter space better, we randomly scan the parameters as the following

$$\begin{aligned} 5 &\leq \tan\beta \leq 50, \quad 0.3 \leq g_X \leq 0.8, \quad 0.01 \leq g_{YX} \leq 0.5, \quad -1 \leq \lambda_C \leq 1, \\ -1 &\leq \lambda_H \leq 1, \quad -2 \text{ TeV} \leq T_{\lambda_C} \leq 2 \text{ TeV}, \quad -2 \text{ TeV} \leq T_{\lambda_H} \leq 2 \text{ TeV}, \\ -5 \text{ TeV} &\leq T_U \leq 5 \text{ TeV}, \quad 4 \text{ TeV}^2 \leq M_Q^2 \leq 8 \text{ TeV}^2, \quad 4 \text{ TeV}^2 \leq M_U^2 \leq 8 \text{ TeV}^2. \end{aligned} \quad (46)$$

In the Fig.2 and Fig.3, ■ denote the lightest CP-even Higgs mass in the region $123 \text{ GeV} \leq m_{h^0} \leq 127 \text{ GeV}$. ● represent the regions $120 \text{ GeV} \leq m_{h^0} < 123 \text{ GeV}$ and $127 \text{ GeV} < m_{h^0} \leq 130 \text{ GeV}$. In the left diagram of Fig.2, the numerical results of m_{h^0} are plotted in the plane of g_X versus g_{YX} . g_X is the gauge coupling constant of the $U(1)_X$ group. g_{YX} is the mixing gauge coupling constant of $U(1)_Y$ group and $U(1)_X$ group. So they should give considerable effects to the results. Most of ■ and ● are concentrated at bottom left part, which form a triangle with two sides as $0.3 \leq g_X \leq 0.55$ and $0 < g_{YX} \leq 0.35$. The points are sparse in the other region. For the right diagram, we show the results of m_{h^0} in the plane of g_X versus λ_C . The points in the region $\lambda_C < 0$ are more than those in the region $\lambda_C > 0$. The concentrated area of ■ and ● is like a rectangle with $-0.1 \geq \lambda_C \geq -0.6$ and $0.3 \leq g_X \leq 0.45$.

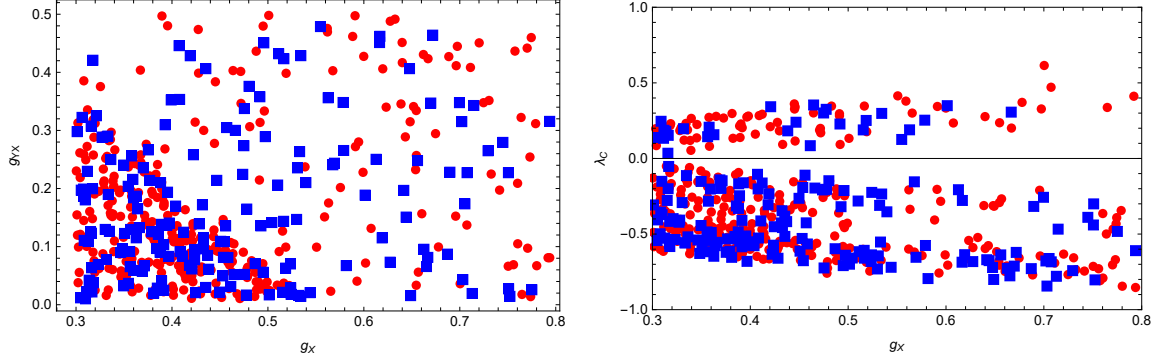


FIG. 2: For the left diagram, the lightest CP-even Higgs mass(m_{h^0}) in the plane of g_X versus g_{YX} ; for the right diagram, m_{h^0} in the plane of g_X versus λ_C .

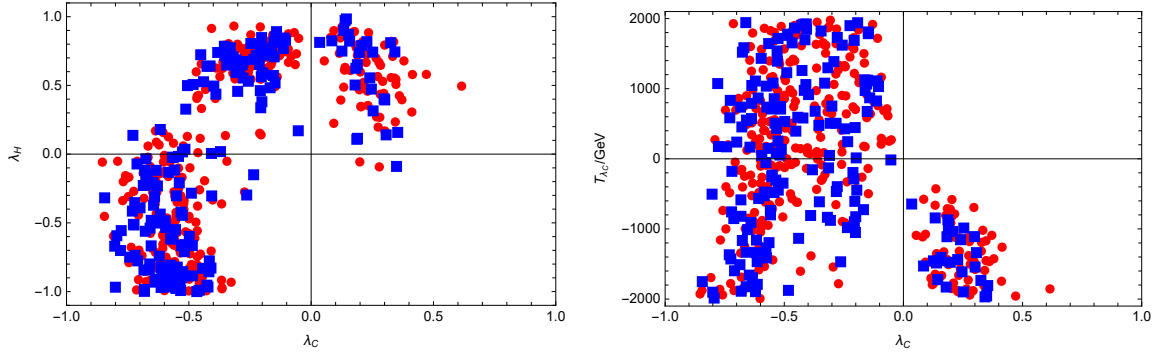


FIG. 3: For the left diagram, m_{h^0} in the plane of λ_C versus λ_H ; for the right diagram, m_{h^0} in the plane of λ_C versus T_{λ_C} .

In the left diagram of Fig.3, m_{h^0} is shown in the plane of λ_C versus λ_H . Many points are in the first, second and third quadrants. In the fourth quadrant, so few points appear. It implies that the second and third quadrants are better for the ■. The numerical results of m_{h^0} versus λ_C and T_{λ_C} are plotted in the right diagram of Fig.3. Obviously, the first quadrant is blank. That is to say, as $\lambda_C > 0$ and $T_{\lambda_C} > 0$, there is not any suitable result. A lot of ■ and ● emerges in the second and third quadrants. In the fourth quadrant, the points concentrate at the lower left corner. From Figs.2 and 3, we can find that λ_C , λ_H and T_{λ_C} are sensitive parameters for m_{h^0} .

The ratio $R_{\gamma\gamma}$ is also researched, and the corresponding results are shown in the Fig.4 and Fig.5, where the notations are ● $\rightarrow 0.95 \leq R_{\gamma\gamma} \leq 1.03$ and ■ $\rightarrow 1.03 < R_{\gamma\gamma} \leq 1.17$. These points ■ and ● satisfy the constraint from m_{h^0} with $120 \text{ GeV} \leq m_{h^0} \leq 130 \text{ GeV}$. The left diagram of Fig.4 embodies $R_{\gamma\gamma}$ in the plane of g_X versus T_u . Many points appear in the

region $0.3 \leq g_X \leq 0.5$, where \bullet concentrate in the T_u range as $-3000 \text{ GeV} \leq T_u \leq 3000 \text{ GeV}$ and \blacksquare are distributed on the upper and lower sides of \bullet . The effects from λ_C and T_u to $R_{\gamma\gamma}$ are studied in the right diagram of Fig.4, where \blacksquare and \bullet are distributed almost the entire area of the graph. \blacksquare mainly appear in the areas above, below, and to the right.

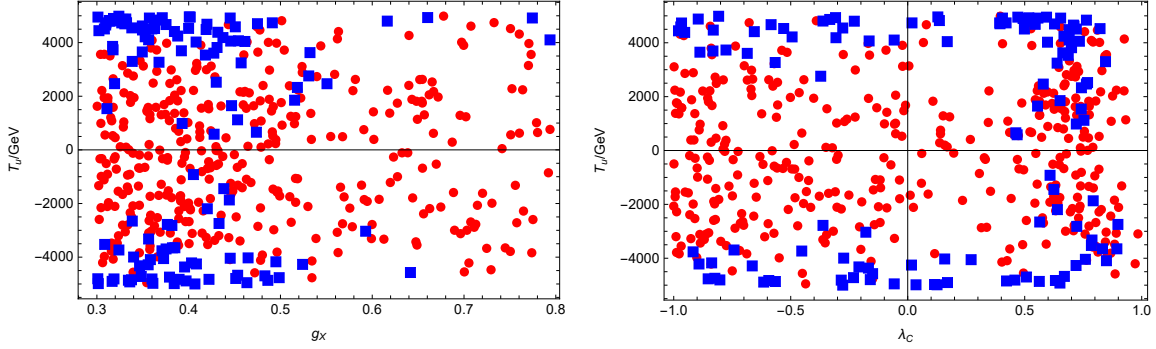


FIG. 4: For the left diagram, $R_{\gamma\gamma}$ in the plane of g_X versus T_u ; for the right diagram, $R_{\gamma\gamma}$ in the plane of λ_C versus T_u .

Both $\tan \beta$ and g_X influence $R_{\gamma\gamma}$, which is shown by the left diagram of Fig.5. It implies that $\tan \beta$ is an insensitive parameter and the effect from $\tan \beta$ is mild. The \blacksquare and \bullet are concentrated in the area $0.3 \leq g_X \leq 0.5$. In the right diagram of Fig.5, the numerical results of $R_{\gamma\gamma}$ are plotted in the plane of M_{QF} versus M_{UF} . M_{QF} and M_{UF} affect scalar quark mass, which affect m_{h^0} and $R_{\gamma\gamma}$. The \bullet are distributed throughout the region of the figure. In the upper right corner, there is almost no \blacksquare . Smaller M_{QF} and M_{UF} produce relative light scalar quarks, which can improve the scalar quark contributions to $R_{\gamma\gamma}$. Therefore, many \blacksquare emerge at the lower left corner.

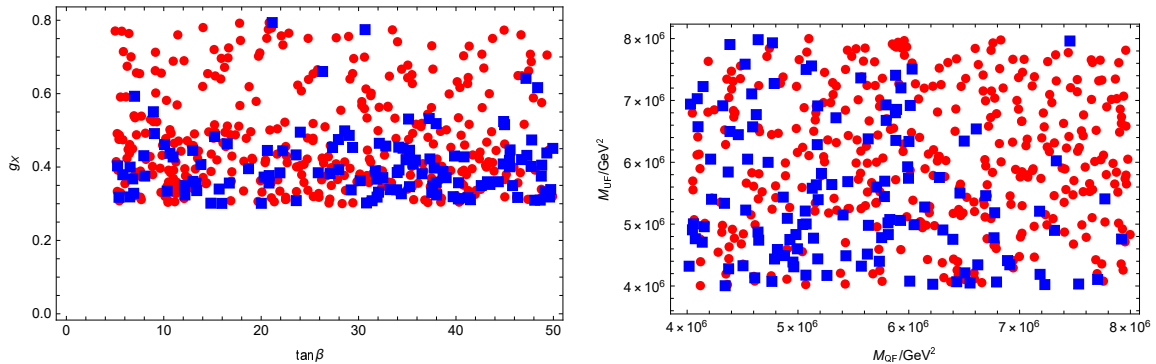


FIG. 5: For the left diagram, $R_{\gamma\gamma}$ in the plane of $\tan \beta$ versus g_X ; for the right diagram, $R_{\gamma\gamma}$ in the plane of M_{QF} versus M_{UF} .

Similarly, we calculate the decays $h^0 \rightarrow WW$ and $h^0 \rightarrow ZZ$. From the numerical results, we find R_{WW} is very close to R_{ZZ} . Therefore, we use R_{VV} (with $V = W, Z$) to denote the both ratios. In the Fig.6, the results of R_{VV} are plotted with \bullet and \blacksquare . Here, \bullet represent $1 \leq R_{VV} \leq 1.03$, and \blacksquare denote $1.03 \leq R_{VV} \leq 1.20$. The left diagram of the Fig.6 shows the relation between R_{VV}, g_X and λ_H . Most \bullet and all \blacksquare are concentrated in the region $0.3 \leq g_X \leq 0.55$, which implies that large g_X is not favourable. The number of \blacksquare is smaller than that of \bullet . For the right diagram, the points concentrate in the region $-1 < \lambda_C < 0$ and $0 < g_{YX} < 0.28$. As $\lambda_C > 0.5$, there is not suitable point. For \blacksquare , the region $-0.7 < \lambda_C < 0$ and $0 < g_{YX} < 0.15$ is advantageous.

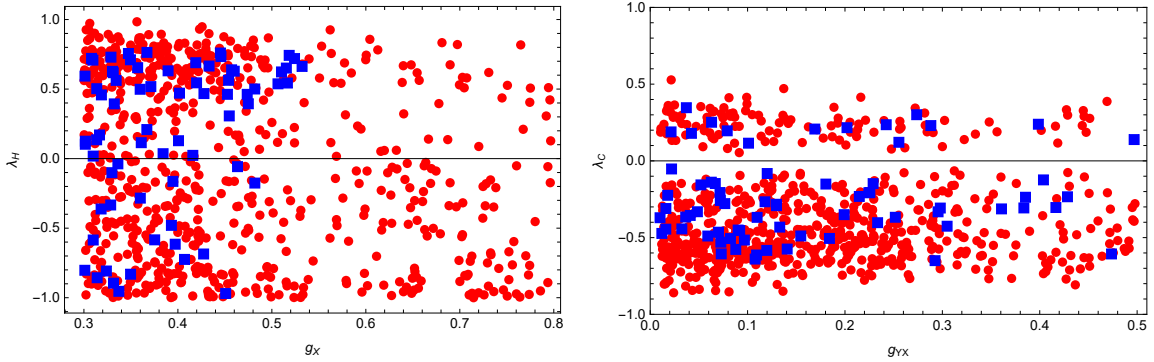


FIG. 6: For the left diagram, R_{VV} (with $V = W, Z$) in the plane of g_X versus λ_H ; for the right diagram, R_{VV} in the plane of g_{YX} versus λ_C .

Here, we study the Higgs decays $h^0 \rightarrow l\bar{l}Z$ and $h \rightarrow \nu_l \bar{\nu}_l Z$ (with $l = e, \mu, \tau$) with the parameters in Eq.(44). The other used parameters are

$$\begin{aligned} \tan \beta &= 10, \quad g_X = 0.37, \quad g_{YX} = 0.1, \quad \lambda_C = -0.1, \\ \lambda_H &= 0.6, \quad T_{\lambda_C} = -0.1 \text{ TeV}, \quad T_{\lambda_H} = 0.3 \text{ TeV}. \end{aligned} \quad (47)$$

After calculation, we obtain the corresponding numerical results in the $U(1)_X SSM$

$$\begin{aligned} Br(h^0 \rightarrow l\bar{l}Z) &= 8.1 \times 10^{-4}, \quad l = e, \mu, \\ Br(h^0 \rightarrow \tau\bar{\tau}Z) &= 8.5 \times 10^{-4}, \\ Br(h^0 \rightarrow \nu_l \bar{\nu}_l Z) &= 1.6 \times 10^{-3}, \quad l = e, \mu, \tau. \end{aligned} \quad (48)$$

For the above decays, the numerical results in Eq.(48) are stable. The authors study these decays in the SM, and give the numerical results as[14]

$$Br(h^0 \rightarrow l\bar{l}Z) = 7.5 \times 10^{-4}, \quad l = e, \mu,$$

$$\begin{aligned}
Br(h^0 \rightarrow \tau\bar{\tau}Z) &= 7.3 \times 10^{-4}, \\
Br(h^0 \rightarrow \nu_l\bar{\nu}_lZ) &= 1.5 \times 10^{-3}, \quad l = e, \mu, \tau.
\end{aligned} \tag{49}$$

Comparing with the ratios in Eq.(49), our numerical results are of the same order and a little bigger than their results. This characteristic should be caused by the new physics contributions. From our numerical research, we find that the processes concerned are attainable in the LHC experiments and may be detected in the near future.

V. DISCUSSION AND CONCLUSION

Introducing three Higgs singlets and right-handed neutrinos to the $U(1)_X$ extension of MSSM, we obtain $U(1)_X$ SSM. In $U(1)_X$ SSM, the neutral CP-even parts of two Higgs doublets(H_d and H_u) and tree Higgs singlets (η , $\bar{\eta}$ and S) mix together, which constitute a 5×5 mass squared matrix of CP-even Higgs. The lightest eigenvalue corresponds to m_{h^0} , but at tree level it can not reach 125 GeV. The loop corrections should be taken into account. In this work, we use the Higgs effective potential with one loop corrections to study the Higgs mass m_{h^0} . The constraint from m_{h^0} near 125 GeV confines the parameter space obviously. The loop corrections from scalar top quark are dominant among the SUSY loop corrections.

The Higgs decays $h^0 \rightarrow \gamma\gamma$ and $h^0 \rightarrow VV$ (with $V = W, Z$) are calculated. The numerical results of the ratios $R_{\gamma\gamma}$ and R_{VV} (with $V = W, Z$) are very near 1. For the researched Higgs decays $h^0 \rightarrow l\bar{l}Z$ (with $l = e, \mu, \tau$), the branching ratios are in the region $(8 \sim 9) \times 10^{-4}$. The branching ratios $R(h^0 \rightarrow \nu_l\bar{\nu}_lZ)$ (with $l = e, \mu, \tau$) are also calculated, whose numerical results are around 1.6×10^{-3} . In the order analysis, these branching ratios are not small, and they are in the detectable range of LHC. We hope that these decays will be detected in the near future, and they benefit the study of Higgs.

Acknowledgments

This work is supported by National Natural Science Foundation of China (NNSFC) (No. 12075074), Natural Science Foundation of Hebei Province (A2020201002, A202201022,

- [1] CMS Collaboration, Phys. Lett. B **716** (2012) 30; ATLAS Collaboration, Phys. Lett. B **716** (2012) 1.
- [2] T2K collaboration, Phys. Rev. Lett. **107** (2011) 041801 [arXiv:1106.2822].
- [3] MINOS collaboration, Phys. Rev. Lett. **107** (2011) 181802 [arXiv:1108.0015].
- [4] J. Rosiek, hep-ph/9511250 [Original paper: Phys. Rev. D **41** (1990) 3464].
- [5] F. Staub, [arXiv: 0806.0538]; Comput. Phys. Commun. **185** (2014) 1773 [arXiv: 1309. 7223].
- [6] S.M. Zhao, T.F. Feng, M.J. Zhang, et al., JHEP **02** (2020) 130 [arXiv: 1905.11007].
- [7] S.M. Zhao, L.H. Su, X.X. Dong, et al., JHEP **03** (2022) 101 [arXiv:2107.03571].
- [8] J.R. Ellis, M.K. Gaillard, D.V. Nanopoulos, Nucl. Phys. B **106** (1976) 292.
- [9] A. Djouadi, Phys. Rep. **459** (2008) 1.
- [10] J.J. Cao, L. Wu, P.W. Wu, et al., JHEP **09** (2013) 043 [arXiv:1301.4641].
- [11] C.H. Chang, T.F. Feng, Y.L. Yan, et al., Phys. Rev. D **90** (2014) 035013 [hep-ph/1401.4586].
- [12] T.F. Feng, S.M. Zhao, H.B. Zhang, et al., Nucl. Phys. B **871** (2013) 223-244.
- [13] R.L. Workman, et al. (Particle Data Group), Prog. Theor. Exp. Phys. **2022** (2022) 083C01.
- [14] Z.Q. Chen, Q.M. Feng, C.F. Qiao, arXiv:2107.04858.
- [15] Q. Qin, Q. Li, C.D. Lü, et al., Eur. Phys. J. C **78** (2018) 10 [arXiv: 1711.07243].
- [16] T.T. Wang, S.M. Zhao, X.X. Dong, et al., JHEP **04** (2022) 122.
- [17] G. Bélanger, J.D. Silva, H.M. Tran, Phys. Rev. D **95** (2017) 115017 [arXiv:1703.03275]; P.H. Chankowski, S. Pokorski, J. Wagner, Eur. Phys. J. C **47** (2006) 187 [hep-ph/0601097].
- [18] S.R. Coleman, Phys. Rev. D **7** (1973) 1888.
- [19] J.H. Kang, P. Langacker, T.J. Li, et al., JHEP **04** (2011) 097 [arXiv: 0911. 2939].
- [20] B. Yan, T.F. Feng, S.M. Zhao, et al., J. Phys. G: Nucl. Part. Phys. **48** (2021) 085003.
- [21] W.Y. Keung, W.J. Marciano, Phys. Rev. D **30** (1984) 248; J.F. Gunion, H.E. Haber, G. Kane, et al., The Higgs Hunter’s Guide, Perseus Books, 1990.
- [22] W. Bernreuther, P. Gonzalez, M. Wiebusch, Eur. Phys. J. C **69** (2010) 31.
- [23] The ATLAS Collaboration, Phys. Lett. B **796** (2019) 68 [arXiv:1903.06248].
- [24] G. Cacciapaglia, C. Csáki, G. Marandella, et al., Phys. Rev. D **74** (2006) 033011; M. Carena, A. Daleo, B.A. Dobrescu, et al., Phys. Rev. D **70** (2004) 093009.

- [25] L. Basso, Adv. High Energy Phys. **2015** (2015) 980687.
- [26] P. Athron, C. Balázs, D.H.J. Jacob, et al., JHEP **09** (2021) 080 [arXiv: 2104.03691].